Engineering Analysis with Boundary Elements 167 (2024) 105871

Contents lists available at ScienceDirect

Engineering Analysis with Boundary Elements

journal homepage: www.elsevier.com/locate/enganabound

Alternating generalized projection method applied to phase-only synthesis process of satellite reflectarray antennas

Rafael Florencio [a,*,1], René Escalante [b,1]

[a] Universidad de Jaén, Departamento de Matemáticas, Jaén, Spain
[b] Universidad de Alcalá, Departamento de Física y Matemáticas, Nonlinear Dynamics and Complex Systems Research Group, Madrid, Spain

ARTICLE INFO

Keywords:
Alternating generalized projection method
Method of alternating projections
Trap points
Intersection on sets
Phase-only synthesis
Intersection approach
Reflectarray antennas
Satellite antennas

ABSTRACT

Promising algorithm of alternating generalized projection method (AGP) is proposed for phase-only synthesis process of satellite reflectarray antennas under intersection approach. This promising algorithm is a hybridized algorithm of two specialized algorithms for non-convex sets rescued in the literature: algorithm based on separating hyperplanes and algorithm based on decomposition method in polar cones. Since the sets involved in phase-only synthesis process of satellite reflectarray antennas are non-convex, the conventional von Neumann alternating projection method proposed in the literature does not guarantee convergence to the point in the intersection of the involved sets. In addition, the results of the phase-only synthesis obtained by the different algorithms were compared and promising improvements produced by the proposed hybridized algorithm were shown.

1. Introduction and preliminaries

The design of broadcast and telecommunication satellite antennas is very challenging due to stringent required electrical and mechanics specifications for space missions [1]. Although during many years shaped surface reflector antennas have been used to satisfy the stringent requirements [2], the last decade reflectarray antennas has been an interesting alternative due to easier and cheaper manufacturing process, low profile and independent control of each polarization [3]. A printed reflectarray antenna consists of a planar array of resonant elements on grounded multilayer substrates illuminated by a feed antenna (typically a feed-horn, see Fig. 1) [3]. The resonant elements scatter the incident electric fields from the feed-horn with a certain phase-shift. For passive reflectarrays (i.e. in absence of active devices connected to reflectarray elements which supplies energy) the scattered electric fields only suffer small energy losses produced by the dielectric support and metallization of the layout (i.e. dielectric and ohmic losses). Since the illumination of the reflectarray is fixed by the feed-horn, magnitude of scattered electric field is mainly fixed by the feed-horn. In this way the phase-shifts produced by each resonant element of reflectarray are the only degrees of freedom to shape the reflected beam. So, the radiated electric field is mainly controlled by these phase-shifts produced by the reflectarray elements. The required value of the phase shift must be determined for each reflectarray element to properly shape the radiating beam and illuminate a specific desired geographic region. The process of the determining these required values of phase-shifts is known as the phase-only synthesis process [3]. Once the values of phase-shift are known, specific lengths of the layout of each resonant element of the reflectarray are varied to produce the required value of phase-shift. The entire process of synthesis and length adjustment is known as the design process [3]. Since the reflectarrays are made resonant elements, the main drawback of the design process is the narrow bandwidth of resonant elements. Fortunately, in last few years significant effort has been done to overcome this limitation [4–7].

Several techniques have been developed to generate shaped beams using planar arrays [8–11]. Concretely, in [11] a comparison between three reflectarray synthesis methods was carried out. Below we show a summary table with the comparison of some synthesis methods:

It has been demonstrated that the phase-only synthesis based on the Intersection Approach [12,13], previously developed for phased arrays, is highly efficient for large reflectarrays [14]. However, according with Table 1 [11], the main drawback of Intersection Approach is that it is very sensitive to initial point (especially for large reflectarrays). In the Intersection Approach technique, two sets are considered: the set of the radiation patterns that can be generated by the reflectarray, and the set of the radiation patterns which satisfy the mission requirements (henceforth $\mathcal{R}$ and $\mathcal{M}$ sets respectively). So, the idea consists of searching for intersection points of the two sets, or at least, a searching for points of each set that are at the minimum distance in a metric space.

* Corresponding author.
E-mail addresses: rfdiaz@ujaen.es (R. Florencio), rene.escalante@uah.es (R. Escalante).
[1] These authors contributed equally to this work.

https://doi.org/10.1016/j.enganabound.2024.105871
Received 29 January 2024; Received in revised form 2 July 2024; Accepted 2 July 2024

Table 1
Comparison between three reflectarray synthesis method shown in [11].

Synthesis method	Brief description	Drawbacks
Synthesis method by beam addition.	This method approximates the desired radiation pattern in the coverage region as superposition of nearby pencil beams.	High sidelobes levels in non-coverage region.
Phase-only synthesis based on gradient techniques method.	A cost function is defined as the distant between the desired radiation pattern and the that produced by the reflectarray for generic phase-shifts. The cost function is minimized by gradient methods.	High computational cost and CPU time for large reflectarrays.
Phase-only synthesis method based on alternating projections (Intersection Approach).	Two sets are defined: set with possible radiated fields by the reflectarray and set with those required in the coverage region. The method tries to find the intersection between both sets by successive projections.	The convergence of the method is very sensitive to initial point (especially with large antennas).

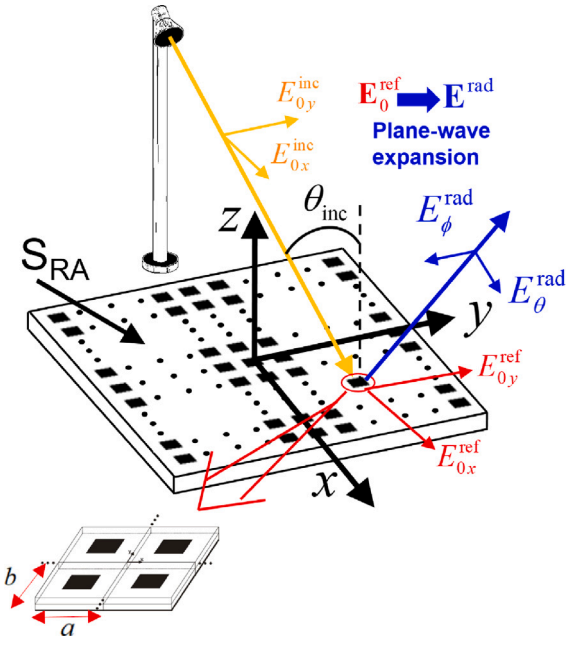

Fig. 1. Scheme of reflectarray antenna of $N_x \times N_y$ elements of $a \times b$ size of the cell. The reflectarray is illuminated by feed-horn. Tangential components of incident and reflected electric field on an specific reflectarray element are shown.

The intersection approach is carried out by means of method of alternating projections (MAP). The sequences generated by MAP, or its extensions, applied by projector operators onto involved sets, in the case of a non-empty intersection, are iteratively applied until convergence to an intersection point (feasible solution) is reached. In the case of an empty intersection it converges to two points (each point in each set) that determine the minimum distance between the sets [15]. MAP, in its simplest formulation, dates back von Neumann [16], who studied the problem of finding the projection of a given point in a Hilbert space onto the intersection of two closed subspaces. Later, this scheme was extended by Cheney and Goldstein [17] to the case of two closed convex sets. Unfortunately, in the reflectarray problem, as we will demonstrate, the sets $\mathcal{R}$ and $\mathcal{M}$ are not convex. In general, when at least one of involved sets is not convex, convergence to the intersection set (if it is not empty) is not guaranteed by the method of projections onto convex sets (POCS) [15]. Fortunately, when non-convex sets are considered, in the known literature some strategies have been proposed (see, for example, [18–21]). This generalized form of MAP, called the alternating generalized projection method (AGP method) [18], was chosen by the authors as the right strategy to face phase-only synthesis.

By applying the AGP method to two non-convex sets, it is expected that the distance between projected and pre-projected points of each set is reduced in each iteration. However, in practice it is possible to detect convergence to pair of points, one of each set, so the distance stops reducing in each iteration. This is a trapping situation, so it is said that we fell into a trap point (any of them). The trap points produce a local minimum of distance between involved sets. In [18] Andrade et al. proposed two different algorithms to leave trap points when two sets are considered, one convex set and other non-convex set. These two proposed algorithms are: algorithm based on separating hyperplanes and algorithm based on decomposition method in polar cones. The results obtained by applying these algorithms were compared with the results obtained by applying the MAP and the two proposed algorithms showed promising results [18].

Therefore, we rescue the two algorithms of AGP proposed in [18] to apply in the intersection approach for phase-only synthesis of satellite reflectarray antennas. Since the sets $\mathcal{R}$ and $\mathcal{M}$ are not convex (as we will show later), we will apply the two algorithms proposed in [18] to our case. We would like to point out that, according with [18], it is expected that the algorithm based on separating hyperplanes generates a convergent sequence to an intersection point of the sets. On the other hand, in [18] the decomposition method based on polar cones is expected to work to leave the trap point. So, in this work not only extensions of the two rescued algorithms are shown, but also hybridized algorithm is proposed. The hybridized algorithm implemented consists of applying the algorithm based on decomposition into polar cones during the first iterations, and after applying the algorithm based on separating hyperplanes for the remaining iterations.

The remainder of the paper is organized as follows. In the next section, a computation process of radiation patterns generated by reflectarray antenna will be shown. This section is required to demonstrate the correct understanding of the radiated electric fields from the reflectarray and the subsequent definitions of the involved sets. After that convexity of the involved sets will be studied in Section 3. These are the set $\mathcal{M}$ of radiated electric fields which satisfy the mission requirements (i.e. it satisfies a given specifications), and the set $\mathcal{R}$ of radiated electric fields which can be generated by the reflectarray. In Section 4 extensions of the rescued algorithms proposed in [18], based on separating hyperplanes and based on decomposition in polar cones, and hybridized algorithm will be shown to face the phase-only synthesis reflectarray in intersection approach technique. In Section 6, a comparison of the numerical results obtained by the algorithms will be presented. Finally in Section 6 some concluding remarks will be presented.

2. Computation of radiation patterns generated by reflectarray antenna

Let us consider the scheme shown in Fig. 1. The scheme shows a reflectarray panel of $N_x \times N_y$ elements arranged in N_x rows and N_y columns where the size of the cell of each element is $a \times b$. In this scheme the reflectarray panel is illuminated by a feed-horn antenna.

Henceforth we will assume that the tangential components of incident electric field generated by the feed-horn, $E_{0x}^{inc}(x, y)$ and $E_{0y}^{inc}(x, y)$, in the plane $z = 0$, on the aperture of the reflectarray panel are known. This assumption is motivated because of wide variety of existing techniques to obtain the tangential components of the electric

field generated by the feed-horn [22–26]. Normally, the feed-horn has a component of the tangential incident electric field whose magnitude is significantly higher than the other component. In that case, it is said that a polarized feed horn is used. For example, when $|E_{0x}^{\text{inc}}(x,y)| \gg |E_{0y}^{\text{inc}}(x,y)|$ then X-polarized feed-horn is used. Henceforth, without loss of generality, we will refer X-polarized feed-horn.

When the components $E_{0x}^{\text{inc}}(x,y)$ and $E_{0y}^{\text{inc}}(x,y)$ are available, the tangential components of the reflected electric field, $E_{0x}^{\text{ref}}(x,y)$ and $E_{0y}^{\text{ref}}(x,y)$ on the reflectarray panel can be computed by solving the scattering problem of the incident electric fields on the resonant elements of the reflectarray panel. Known numerical tools—such as finite element (FE) [27], finite difference time domain (FDTD) [28], and method of moments (MM) [29] are suitable to solve this scattering problem. Since this scattering problem involves large structures made of resonant elements, high computational resources are usually required for solving the scattering problem with acceptable accuracy. In order to reduce computational cost, it is preferable boundary element approach of the scattering problem as techniques based on MM. For example, in [30] MM scheme with Fast Fourier Transform (FFT) and Biconjugate Gradient Stabilized method (BICGSTAB) is proposed to solve the scattering problem of the incident electric field on large reflectarray panel.

Either way, the components $E_{0x}^{\text{ref}}(x,y)$ and $E_{0y}^{\text{ref}}(x,y)$ of the reflected electric field can be obtained from the components $E_{0x}^{\text{inc}}(x,y)$ and $E_{0y}^{\text{inc}}(x,y)$ of the tangential incident electric field in plane $z=0$, on the reflectarray panel. In reflectarray antenna designs, usually the polarization of the incident electric field from the feed-horn is kept in the produced reflected electric field. So, if X-polarized feed-horn is used, then X-polarized reflectarray is usually desired (i.e. If $|E_{0x}^{\text{inc}}(x,y)| \gg |E_{0y}^{\text{inc}}(x,y)|$ then $|E_{0x}^{\text{ref}}(x,y)| \gg |E_{0y}^{\text{ref}}(x,y)|$ is desired). Moreover, we would like to point out that, for passive elements of the reflectarray (i.e. reflectarray elements that are not coupled to active devices such as diodes, transistors, etc, that supply energy) the magnitude of the more significant component of the tangential reflected electric field is always less or equal to the magnitude of the more significant component of the tangential incident electric field (i.e. $|E_{0x}^{\text{ref}}(x,y)| \leq |E_{0x}^{\text{inc}}(x,y)|$ for X-polarized reflectarray antennas). We will revisit this topic once the convexity of the set $\mathcal{R}$ has been studied.

Once the tangential components of the reflected electric fields in the plane $z=0$ are available, the spherical angular components of the radiated electric field can be obtained by [25]:

$$E_{\theta}^{\text{rad}}(r,\theta,\phi) = \frac{jk_0}{2\pi r} e^{-jk_0 r}\left[\cos(\phi)\widetilde{E}_{0x}^{\text{ref}}(u,v) + \sin(\phi)\widetilde{E}_{0y}^{\text{ref}}(u,v)\right] \tag{1}$$

$$E_{\phi}^{\text{rad}}(r,\theta,\phi) = \frac{jk_0 e^{-jk_0 r}}{2\pi r}\cos(\theta)\left[\cos(\phi)\widetilde{E}_{0y}^{\text{ref}}(u,v) - \sin(\phi)\widetilde{E}_{0x}^{\text{ref}}(u,v)\right] \tag{2}$$

where j is the imaginary unit and where $u = \sin(\theta)\cos(\phi), v = \sin(\theta)\cos(\phi)$. The observation points with respect to the reference system shown in Fig. 1 are described by their spherical components (r,θ,ϕ) with $r \gg \frac{2\pi}{k_0}$. The functions $\widetilde{E}_{0x}^{\text{ref}}(u,v)$ and $\widetilde{E}_{0y}^{\text{ref}}(u,v)$ are the angular spectrum of plane waves of the tangential components of the reflected electric fields $E_{0x}^{\text{ref}}(x,y)$ and $E_{0y}^{\text{ref}}(x,y)$ [25]:

$$\widetilde{E}_{0x/y}^{\text{ref}}(u,v) = \int_{-\infty}^{\infty}\int_{-\infty}^{\infty} E_{0x/y}^{\text{ref}}(x,y)e^{jk_0(ux+vy)}\,dx\,dy \tag{3}$$

Note that (3) is not strictly a Fourier Transform of $E_{0x/y}^{\text{ref}}(x,y)$ since $u^2+v^2 \leq 1$. This fact is imposed because the angular spectrum of plane waves only take into account the continuous contribution of electric fields $E_{0x/y}^{\text{ref}}(x,y)e^{jk_0(ux+vy)}$ of plane waves with real propagation constant $\mathbf{k} = k_x\hat{\mathbf{x}} + k_y\hat{\mathbf{y}} + k_z\hat{\mathbf{z}}$, with magnitude $|\mathbf{k}| \leq k_0$. We would like to point out that the magnitude of $E_{0x/y}^{\text{ref}}(x,y)$ is neglected on the outside region of reflectarray panel in 'x' and 'y' directions. In fact, the limits of integration shown in (3) are reduced to the surface, S_{RA} (see Fig. 1), of reflectarray panel in $z=0$. In this way, the spectrum of plane waves is usually approximated by:

$$\widetilde{E}_{0x/y}^{\text{ref}}(u,v) \approx \iint_{S_{\text{RA}}} E_{0x/y}^{\text{ref}}(x,y)e^{jk_0(ux+vy)}\,dx\,dy \tag{4}$$

Moreover, since we assume X-polarized reflectarray (i.e. $|E_{0x}^{\text{ref}}(x,y)| \gg |E_{0y}^{\text{ref}}(x,y)|$) the y-component of the tangential reflected electric field can be neglected. Consequently, its angular spectrum of plane waves $\widetilde{E}_{0y}^{\text{ref}}(u,v)$ is also neglected. In this way, the spherical angular components of the radiated electric field given in (1) and (2) can be approximated by:

$$E_{\theta}^{\text{rad}}(r,\theta,\phi) \approx \frac{jk_0}{2\pi r} e^{-jk_0 r}\cos(\phi)\widetilde{E}_{0x}^{\text{ref}}(u,v) \tag{5}$$

$$E_{\phi}^{\text{rad}}(r,\theta,\phi) \approx -\frac{jk_0 e^{-jk_0 r}}{2\pi r}\cos(\theta)\sin(\phi)\widetilde{E}_{0x}^{\text{ref}}(u,v) \tag{6}$$

The spectrum of plane waves $\widetilde{E}_{0x}^{\text{ref}}(u,v)$ can be computed by (4) in an efficient manner by means of a partition of the S_{RA} into $N \times M$ cells of size, $a \times b$, with $M = N = 2^k, k \in \mathbb{N}$ in order to apply the Fast Fourier Transform Algorithm (FFT Algorithm) [31] (see [3] for more details).

For pass from the cartesian variables u-v to the angular spherical variables we can use the known change variables:

$$\theta = \arcsin(\sqrt{u^2+v^2}) \tag{7}$$

$$\phi = \begin{cases} \arctan\left(\frac{v}{u}\right) & \text{if } u > 0 \\ \frac{\pi}{2} & \text{if } u = 0,\ v > 0 \\ \pi + \arctan\left(\frac{v}{u}\right) & \text{if } u\langle 0,\ v\rangle 0 \\ -\frac{\pi}{2} & \text{if } u = 0,\ v < 0 \\ -\pi + \arctan\left(\frac{v}{u}\right) & \text{if } u\langle 0,\ v\rangle 0 \end{cases} \tag{8}$$

The Eqs. (5) and (6) provide the spherical angular components of the radiated electric field. In the computation of radiation patterns, it is common to use co-polar and cross-polar components according to third Ludwig definition [32]. For X-polarized reflectarray antenna, the transformation from spherical angular components, E_{θ}^{rad} and E_{ϕ}^{rad}, of the radiated electric field to co-polar and cross-polar components, $E_{\text{cp}}^{\text{rad}}$ and $E_{\text{xp}}^{\text{rad}}$, are given by:

$$\begin{pmatrix} E_{\text{cp}}^{\text{rad}}(r,\theta,\phi) \\ E_{\text{xp}}^{\text{rad}}(r,\theta,\phi) \end{pmatrix} = \begin{pmatrix} \cos(\phi) & -\sin(\phi) \\ -\sin(\phi) & -\cos(\phi) \end{pmatrix}\begin{pmatrix} E_{\theta}^{\text{rad}}(r,\theta,\phi) \\ E_{\varphi}^{\text{rad}}(r,\theta,\phi) \end{pmatrix} \tag{9}$$

From the radiated co-polar electric field component, we can compute the co-polar gain of the reflectarray antenna with respect to the input power of the feed-horn. This gain is defined as ratio between the density power per unit area produced by the radiated co-polar electric field component and the density power per unit area of an isotropic source with input power equal to feed-horn power [3]:

$$G_{\text{cp}}(\theta,\phi) = \frac{\left|E_{\text{cp}}^{\text{rad}}(r,\theta,\phi)\right|^2 4\pi r^2}{2\eta P_{\text{Feed}}} \tag{10}$$

Where η is the vacuum impedance and P_{Feed} is the power of the feed-horn. Please, note that the dependence with 'r' variable disappear in (10). This fact can be shown by substituting (9), (5) and (6) in (10):

$$G_{\text{cp}}(\theta,\phi) = \frac{k_0^2}{2\pi\eta P_{\text{Feed}}}\left|\widetilde{E}_{0x}^{\text{ref}}(u,v)\right|^2 \left[\cos^2(\phi) + \sin^2(\phi)\cos(\theta)\right]^2 \tag{11}$$

3. Study of convexity of involved sets $\mathcal{M}$ and $\mathcal{R}$

In this section we will study the convexity of the involved sets $\mathcal{M}$ (set of the radiation patterns which satisfy the mission requirements) and $\mathcal{R}$ (set of the radiation patterns that can be generated by the reflectarray).

Let us begin with the set $\mathcal{M}$. This set contains the radiated electric fields that satisfies requirements of the gain in specific coverage region. These requirements of gain of satellite antenna missions are usually given as required minimum and maximum gain, $g_{\text{cp}}^{\min}(u,v)$ and $g_{\text{cp}}^{\max}(u,v)$ on coverage region of radiation pattern diagram. The gain of the co-polar component of the radiated electric field should fulfill $g_{\text{cp}}^{\min}(u,v) \leq$

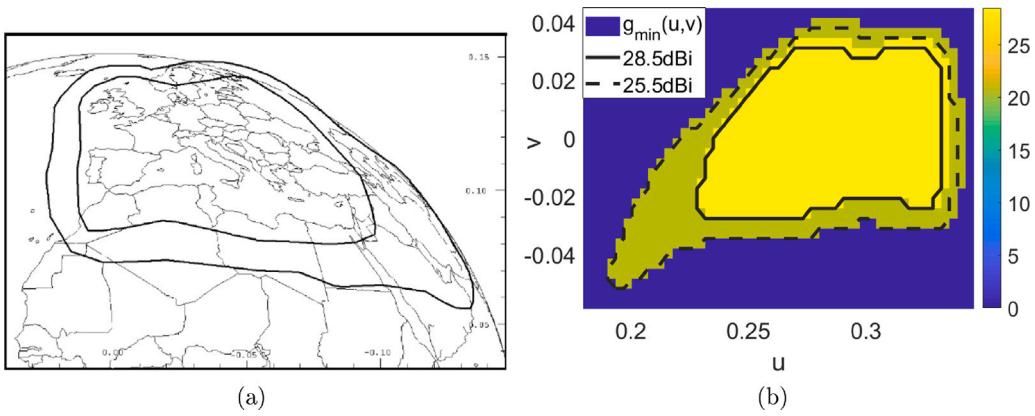

Fig. 2. (a) Contour of Europe coverage seen from 5° west orbital position; (b) Minimum gain requirements in the defined coverage [14].

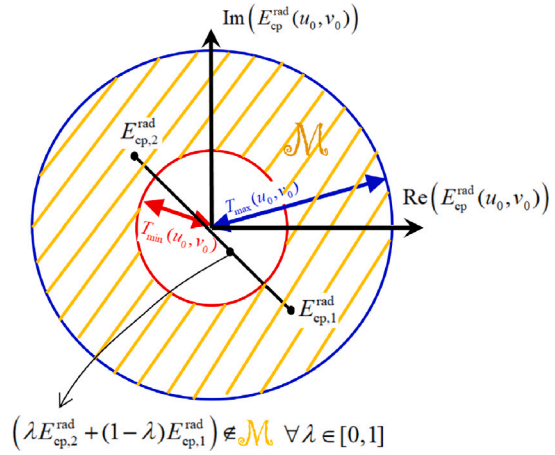

Fig. 3. Set $\mathcal{M}$ defined by (14) is shown in complex plane for fixed values of $u = u_0, v = v_0$. The set $\mathcal{M}$ is not convex since the line segment joining points $E^{\text{rad}}_{\text{cp},1}(u,v)$ and $E^{\text{rad}}_{\text{cp},2}(u,v)$ is not completely within the set $\mathcal{M}$.

$G_{\text{cp}}(u,v) \leq g^{\max}_{\text{cp}}(u,v)$. Examples of mission requirements on coverage is given in Fig. 2 [14]:

From $g^{\min}_{\text{cp}}(u,v)$ and $g^{\max}_{\text{cp}}(u,v)$ and (10), we can define the maximum and minimum values of the magnitude of the co-polar component of the radiated electric field which satisfies the mission requirements:

$$T_{\max}(u,v) = \sqrt{\frac{g^{\max}_{\text{cp}}(u,v)\eta P_{\text{Feed}}}{4\pi r^2}} \tag{12}$$

$$T_{\min}(u,v) = \sqrt{\frac{g^{\min}_{\text{cp}}(u,v)\eta P_{\text{Feed}}}{4\pi r^2}} \tag{13}$$

So, we can define the set $\mathcal{M}$ of radiated electric fields that satisfy the mission requirements as those with a co-polar component that satisfies:

$$\mathcal{M} \equiv \left\{ E^{\text{rad}}_{\text{cp}} \in \mathbb{C} : T_{\min} \leq \left| E^{\text{rad}}_{\text{cp}} \right| \leq T_{\max} \right\} \tag{14}$$

In Fig. 3 the set $\mathcal{M}$ defined by (14) is shown in complex plane for fixed values of $u = u_0, v = v_0$. The set consists of a ring which is limited by circumferences of radius $T_{\min}(u_0,v_0)$ and $T_{\max}(u_0,v_0)$. Let us define convex set in complex plane:

Definition 1. Let us $\mathcal{M} \subseteq \mathbb{C}$. $\mathcal{M}$ is a convex set if $\lambda x + (1-\lambda)y \in \mathcal{M}$ $\forall x, y \in \mathcal{M}$ and $\forall \lambda \in [0,1]$.

The Definition 1 defines a convex set as a set where, for two points of the set, x and y, the line segment joining points x and y lies completely within the set. According with Fig. 3, is clear that the set $\mathcal{M}$ is not convex since the line segment joining points $E^{\text{rad}}_{\text{cp},1}(u,v)$ and $E^{\text{rad}}_{\text{cp},2}(u,v)$ is not completely within the set $\mathcal{M}$.

Now, let us consider the set $\mathcal{R}$. If we revisit the previous section, taking into account (4), (5), and (6) when formulating (9), the co-polar component of radiated electric field generated by the reflectarray can be obtained from x-component of the reflected electric field as following:

$$E^{\text{rad}}_{\text{cp}}(r,\theta,\phi) = jk_0 \frac{e^{-jk_0 r}}{2\pi r}\left[\cos^2(\phi) + \sin^2(\phi)\cos(\theta)\right] \tag{15}$$
$$\iint_{S_{\text{RA}}} E^{\text{ref}}_{0x}(x,y) e^{jk_0(ux+vy)} dxdy$$

According with Section 2, for passive elements of the X-polarized reflectarray antenna is satisfied that $|E^{\text{ref}}_{0x}(x,y)| \leq |E^{\text{inc}}_{0x}(x,y)|$. This fact is because losses of power is produced by the lossy dielectric material and ohmic losses of metallizations of the reflectarray element. Since dielectric material with low dielectric loss and good conductors with low ohmic losses are previously selected, it is expected that $|E^{\text{ref}}_{0x}(x,y)| \approx |E^{\text{inc}}_{0x}(x,y)|$. The strict equality between the magnitudes the reflected and incident electric fields, $|E^{\text{ref}}_{0x}(x,y)| = |E^{\text{inc}}_{0x}(x,y)|$, is only produced for ideal non-lossy dielectric material and ideal metallizations without ohmic losses. The argument of $E^{\text{ref}}_{0x}(x,y)$ is the argument of $E^{\text{inc}}_{0x}(x,y)$ plus the phase-shift, $\varphi(x,y)$, generated by the reflectarray element (i.e. $\arg(E^{\text{ref}}_{0x}(x,y)) = \arg(E^{\text{inc}}_{0x}(x,y)) + \varphi(x,y)$). So, we can define the $\mathcal{R}$ set of radiated electric fields which can be generated by the reflectarray as the radiated electric fields with co-polar component which satisfies:

$$\mathcal{R} \equiv \{ E^{\text{rad}}_{\text{cp}} \in \mathbb{C} : \exists \varphi(x,y) \in \mathbb{R} \text{ with} \tag{16}$$
$$E^{\text{rad}}_{\text{cp}} = jk_0 \frac{e^{-jk_0 r}}{2\pi r}\left[\cos^2(\phi) + \sin^2(\phi)\cos(\theta)\right]$$
$$\iint_{S_{\text{RA}}} \left| E^{\text{inc}}_{0x}(x,y) \right| e^{j[\arg(E^{\text{inc}}_{0x}(x,y)) + \varphi(x,y)]} e^{jk_0(ux+vy)} dxdy \}$$

where $E^{\text{inc}}_{0x}(x,y)$ is fixed by the feed-horn of the reflectarray antenna. According with Definition 1, we can check that the $\mathcal{R}$ set is not convex. Let us $E^{\text{rad}}_{\text{cp},1}$, $E^{\text{rad}}_{\text{cp},2} \in \mathcal{R}$ produced from $E^{\text{ref}}_{0x,1}(x,y), E^{\text{ref}}_{0x,2}(x,y)$ such that $|E^{\text{ref}}_{0x,k}(x,y)| = |E^{\text{inc}}_{0x,k}(x,y)|$ and $\arg(E^{\text{ref}}_{0x,k}(x,y)) = \arg(E^{\text{inc}}_{0x}(x,y)) + \varphi_k(x,y)$, $k = 1,2$. Let us check that the line segment joining points $E^{\text{rad}}_{\text{cp},1}$ and $E^{\text{rad}}_{\text{cp},2}$ is not completely within the set $\mathcal{R}$. First, we compute the amount $E^{\text{rad}}_{\text{cp},2} + (1-\lambda)E^{\text{rad}}_{\text{cp},1} \forall \lambda \in [0,1]$:

$$\lambda E^{\text{rad}}_{\text{cp},2} + (1-\lambda)E^{\text{rad}}_{\text{cp},1} = jk_0 \frac{e^{-jk_0 r}}{2\pi r}\left[\cos^2(\phi) + \sin^2(\phi)\cos(\theta)\right] \tag{17}$$
$$\iint_{S_{\text{RA}}} \left| E^{\text{inc}}_{0x}(x,y) \right| \left[\lambda e^{j\arg(E^{\text{ref}}_{0x,2}(x,y))} + (1-\lambda) e^{j\arg(E^{\text{ref}}_{0x,1}(x,y))} \right] e^{jk_0(ux+vy)} dxdy$$

Since the term of square bracket, $\lambda e^{j\arg(E^{\text{ref}}_{0x,2}(x,y))} + (1-\lambda) e^{j\arg(E^{\text{ref}}_{0x,1}(x,y))}$, is not a complex number with unitary magnitude in general, then

$\nexists\varphi(x,y)\in\mathbb{R}$ such that

$$\lambda E^{\text{rad}}_{\text{cp},2}+(1-\lambda)E^{\text{rad}}_{\text{cp},1}=\ jk_0\frac{e^{-jk_0r}}{2\pi r}\left[\cos^2(\phi)+\sin^2(\phi)\cos(\theta)\right] \tag{18}$$
$$\iint_{S_{\text{RA}}}\left|E^{\text{inc}}_{0x}(x,y)\right|e^{j[\arg(E^{\text{inc}}_{0x}(x,y))+\varphi(x,y)]}e^{jk_0(ux+vy)}dxdy,\ \ \forall\lambda\in[0,1]$$

So, $(\lambda E^{\text{rad}}_{\text{cp},2}+(1-\lambda)E^{\text{rad}}_{\text{cp},1})\notin\mathcal{R}\forall\lambda\in[0,1]$. Therefore, $\mathcal{R}$ set is not convex.

Please note that, unlike the set $\mathcal{M}$, representing the set $\mathcal{R}$ graphically is complicated because the elements of $\mathcal{R}$ involve the functions $E^{\text{ref}}_{0x}(x,y)$.

4. Trap points and how to avoid them

According with (11) and (4), the synthesis of radiation pattern for reflectarray antennas requires obtaining of the tangential components of reflected electric field on reflectarray panel. More concretely, it is required the determining of the argument, $\arg(E^{'\text{,ref}}_{0x}(x,y))$, of x-component of the reflected electric field.

This synthesis process can be approached as a search for intersection points of two sets, or at least, a search for points of each set that are at the minimum distance in a metric spaces. These sets are given by (14) as the $\mathcal{M}$ set of radiated electric fields which satisfy the mission requirements and by (16) as the $\mathcal{R}$ set of radiated electric fields which can be generated by the reflectarray. This approach of searching for intersection points of the two sets is known as "intersection approach" in reflectarray antenna synthesis [3,12,13]. The intersection approach is carried out by means of method of alternating projections (MAP). In MAP sequences that involves projector operators on involved sets are iteratively applied in order to converge to intersection points (feasible solution) or points of each set that are at the minimum distance in a metric space.

Maybe, the more known MAP is the von Neumann's scheme [16]. This scheme was extended by Cheney and Goldstein [17] for convex sets. This scheme is based on following theorem:

Theorem 1. *Let us two closed convex sets A, B of Hilbert Space $\mathcal{H}$, with projector operators P_A and P_B respectively. Let us $x_0\in\mathcal{H}$. Then* $\lim_{k\to\infty}\left(P_BP_A\right)^k x_0=P_{A\cap B}x_0$

Note that, according with Theorem 1, the knowledge of projector operators are required to implement an algorithm based on Theorem 1. In our case, the projector operator can be defined for the sets $\mathcal{M}$ and $\mathcal{R}$ as following:

Definition 2. Let us $\mathcal{M}\subseteq\mathbb{C}$ as $\mathcal{M}\equiv\left\{E^{\text{rad}}_{\text{cp}}(u,v)\in\mathbb{C}:T_{\min}(u,v)\le\left|E^{\text{rad}}_{\text{cp}}(u,v)\right|\le T_{\max}(u,v)\right\}$ and consider $E'^{\text{rad}}_{\text{cp}}(u,v)\in\mathbb{C}$. The projector operator $P_{\mathcal{M}}$ on set $\mathcal{M}$ is defined as:

$$P_{\mathcal{M}}(E'^{\text{rad}}_{\text{cp}}(u,v))=\begin{cases}T_{\max}(u,v)e^{j\arg(E'^{\text{rad}}_{\text{cp}}(u,v))}\ if\ T_{\max}(u,v)\le\left|E'^{\text{rad}}_{\text{cp}}(u,v)\right|\\ T_{\min}(u,v)e^{j\arg(E'^{\text{rad}}_{\text{cp}}(u,v))}\ if\ T_{\min}(u,v)\ge\left|E'^{\text{rad}}_{\text{cp}}(u,v)\right|\\ E'^{\text{rad}}_{\text{cp}}(u,v)\ if\ T_{\min}(u,v)\le\left|E^{\text{rad}}_{\text{cp}}(u,v)\right|\le T_{\max}(u,v)\end{cases} \tag{19}$$

Note that this projector operator only modifies the modulus of complex number of $E^{'\text{,rad}}_{\text{cp}}(u,v)$ if $E^{'\text{,rad}}_{\text{cp}}(u,v)\notin\mathcal{M}$, but the argument, $\arg(E^{'\text{,rad}}_{\text{cp}}(u,v))$, is kept.

According with (16), next we define the projector operator $P_{\mathcal{R}}$ on set $\mathcal{R}$.

Definition 3. Let us consider

$\mathcal{R}\subseteq\mathbb{C}\ as\mathcal{R}\equiv\{E^{\text{rad}\in}_{\text{cp}}\mathbb{C}:$

$$E^{\text{rad}}_{\text{cp}}=jk_0\frac{e^{-jk_0r}}{2\pi r}\left[\cos^2(\phi)+\sin^2(\phi)\cos(\theta)\right]$$
$$\iint_{S_{\text{RA}}}\left|E^{\text{inc}}_{0x}(x,y)\right|e^{j\arg(E^{\text{ref}}_{0x}(x,y))}e^{jk_0(ux+vy)}dxdy\}$$

and $E'^{\text{rad}}_{\text{cp}}(u,v)\in\mathbb{C}:\exists E^{'\text{,ref}}_{0x}(x,y)\in\mathbb{C}$:

$$E'^{\text{,rad}}_{\text{cp}}(u,v)=jk_0\frac{e^{-jk_0r}}{2\pi r}\left[\cos^2(\phi)+\sin^2(\phi)\cos(\theta)\right] \tag{20}$$
$$\iint_{S_{\text{RA}}}E^{'\text{,ref}}_{0x}(x,y)e^{jk_0(ux+vy)}dxdy$$

and $E^{\text{inc}}_{0x}(x,y)\in\mathbb{C}$. Then the projector operator $P_{\mathcal{R}}$ on set $\mathcal{R}$ is defined as:

$$P_{\mathcal{R}}(E'^{\text{,rad}}_{\text{cp}}(u,v))=jk_0\frac{e^{-jk_0r}}{2\pi r}\left[\cos^2(\phi)+\sin^2(\phi)\cos(\theta)\right] \tag{21}$$
$$\iint_{S_{\text{RA}}}\left|E^{\text{inc}}_{0x}(x,y)\right|e^{j\arg(E^{'\text{,ref}}_{0x}(x,y))}e^{jk_0(ux+vy)}dxdy$$

Note that this projector operator replaces the modulus of complex number of the integrand $E^{'\text{,ref}}_{0x}(x,y)$ by the modulus of the complex number of the incident electric field $E^{\text{inc}}_{0x}(x,y)$.

Once the projector operators are defined, the von Neumann's algorithm can be applied to the sets $\mathcal{M}$ and $\mathcal{R}$. The following algorithm given in Table 2 is proposed from the theorem particularized for the sets $\mathcal{M}$ and $\mathcal{R}$. Also, flowchart of the algorithm is shown in Fig. 4. The proposed algorithm uses as initial point a $E^{\text{rad}}_{\text{cp}}\in\mathcal{M}$. This selection is carried out because of the ease to choose a co-polar component of the radiated electric field which satisfy the mission requirements (for example: $E^{\text{rad}}_{\text{cp}}(u,v)=T_{\min}(u,v)$)

Note that, according to Theorem 1, if feasible solution exists, then convergence to intersection point is guaranteed when the involved sets are closed convex sets. Although the theorem does not state anything when there is not intersection point (i.e. feasible solution does not exist), it is known that the algorithm reaches the convergence to points of each set that are at the minimum distance [18]. However, this algorithm cannot guarantee convergence to a feasible solution if any of the sets is non-convex. In fact, when non-convex sets are considered, a generalized form of MAP is used. These generalized form of MAP are usually called as alternating generalized projection method (AGP) [18].

When two non-convex sets are considered, it is expected that the distance between projected and pre-projected points of each set is reduced in each iteration of applying AGP method in a metric spaces. However, in practice it is possible to detect convergence to pair of points, one of each set, whose the distance is not reduced in each iteration. One of pair of points is called trap points. The trap points are characterized by following properties:

1. Let us A,B sets being any non-convex set. Let us define the function $J(x)=d(x,B)\equiv\inf_{y\in B}\|x-y\|$ with $x\in A$. Then x is a trap point if it is a local minimum of $J(\cdot)$ and $J(x)>0$.
2. The convergence to a trap point depends strongly on the initial point (see Fig. 5).

Table 2
Von Neumann algorithm (MAP).

Algorithm 1: von Neumann's method

Require $E^{\text{rad}}_{\text{cp},0}\in\mathcal{M}$, ε = tolerance, N_T := maximum number of iterations
for $k:=0,\ 1,\ 2,\ldots,N_T$ **do**
  $E^{\text{rad}}_{\text{cp},k+1}=P_{\mathcal{M}}\left(P_{\mathcal{R}}\left(E^{\text{rad}}_{\text{cp},k}\right)\right)$
  $J\left(E^{\text{rad}}_{\text{cp},k}\right)=\left\|P_{\mathcal{R}}\left(E^{\text{rad}}_{\text{cp},k}\right)-E^{\text{rad}}_{\text{cp},k+1}\right\|$
  if $J(E^{\text{rad}}_{cp,k+1})<\varepsilon$
    return $E^{\text{rad}}_{\text{cp},k}$
    Stop, the algorithm converges to a point in $\mathcal{M}\cap\mathcal{R}$
  end if
end for

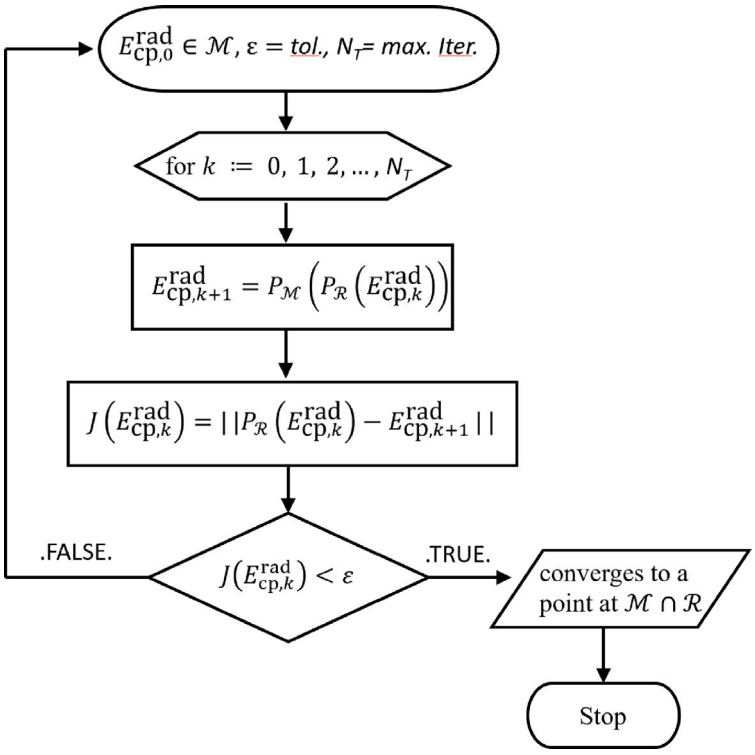

Fig. 4. Flowchart of the von Neumann's algorithm (algorithm 1 given in Table 2).

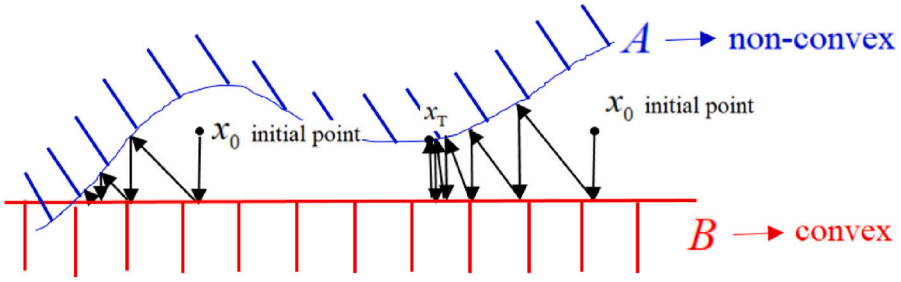

Fig. 5. Example of two sets A, B with A non-convex set and B convex set. The convergence to a trap point x_T depends strongly of the initial point.

According with previous section, $\mathcal{M}$ and $\mathcal{R}$ sets are not convex. So, there is not guaranteed convergence to feasible solution (or convergence to points of each set that are at the minimum distance if feasible solution does not exist) by application of MAP. Therefore, AGP methods should be implemented in order to leave from trap points. With this purpose, we rescue two algorithms of AGP proposed in [18]. One algorithm is based on sequence of separating hyperplanes while that, another algorithm is based on decomposition method in polar cones. In next subsections these algorithm will be briefly described and we will adapt them for reflectarray antenna synthesis.

4.1. Algorithm based on separating hyperplanes

This algorithm was proposed in [18] where a non-convex set, A, and other convex set, B, and their projector operators P_A and P_B, were considered. It is a known results that, given a point $x \notin B$, there exist a separating hyperplane H that separates x and B. In [18] the following process was proposed: given a point x_i, the projected point on B, $P_B(x_i)$ is obtained. Next, a point w_i is selected in the line segment joining the points x_i and $P_B(x_i)$ (for example $w_i = (x_i + P_B(x_i))/2$). Then, the separating hyperplane H_i is define as the hyperplane containing the point w_i, whose normal vector is the gradient vector of B in the point $P_B(x_i)$. It is expected that the intersection between the separating hyperplane H_i and non-convex set A is non-empty set (i.e. $H_i \cap A \neq \emptyset$). Let us consider $x_{H_i \cap A} \in H_i \cap A$. The existence of $x_{H_i \cap A}$ is guaranteed as long as the point w_i exists such as $H_i \cap A \neq \emptyset$. If the point $x_{i+1} = x_{H_i \cap A} \notin B$ other hyperplane H_{i+1} that separates x_{i+1} and B is computed in order to obtain an intersection point $x_{i+2} = x_{H_{i+1} \cap A} \in H_{i+1} \cap A$. So, a sequences of points $\{x_i\}_{i \geq 0}$ and hyperplanes $\{H_i\}_{i \geq 0}$ are generated such that $x_{i+1} \in H_{i+1} \cap A$. In [18] it is expected that this sequence of points $\{x_i\}_{i \geq 0}$ converges to a point in the intersection $A \cap B$. In fact, numerical results with promising results were shown in [18] (see Table 4 of results of experiment 3 in [18]). We extend the proposed algorithm in [18] to face reflectarray antenna synthesis. The following points describe this extension considering fixed values of u, v:

1. Since $E^{rad}_{cp} = (\mathrm{Re}(E^{rad}_{cp}) + j\mathrm{Im}(E^{rad}_{cp})) \in \mathbb{C}$, we will consider $(\mathrm{Re}(E^{rad}_{cp}), \mathrm{Im}(E^{rad}_{cp})) \in \mathbb{R}^2$ with conventional Euclidean inner product.
2. We will consider $\mathcal{M}$ and $\mathcal{R}$ sets defined in (14) and (16). We remember that they are non-convex sets and for this reason, this is an extension of the algorithm.
3. Let us $E^{rad}_{cp,i} = P_{\mathcal{M}}(P_{\mathcal{R}}(E^{rad}_{cp,i-1})) = E^{rad}_{cp,T} \in \mathcal{M}$ a trap point. We define $w_{\mathcal{R},i} = (P_{\mathcal{R}}(E^{rad}_{cp,i-1}) + E^{rad}_{cp,i-1})/2$ and $w_{\mathcal{M},i} = (E^{rad}_{cp,i} + P_{\mathcal{R}}(E^{rad}_{cp,i-1}))/2$.

Table 3
AGP based on separating hyperplanes.

Algorithm 2: AGP based on separating hyperplanes

Require $E^{\text{rad}}_{\text{cp},0} \in \mathcal{M}$, ε = tolerance, N_T := maximum number of iterations
for $k := 0,\ 1,\ 2, \ldots, N_T$ **do**
  $E^{\text{rad}}_{\text{cp},k+1} = P_{\mathcal{M}}\left(P_{\mathcal{R}}\left(E^{\text{rad}}_{\text{cp},k}\right)\right)$
  $J\left(E^{\text{rad}}_{\text{cp},k}\right) = \left\| P_{\mathcal{R}}\left(E^{\text{rad}}_{\text{cp},k}\right) - E^{\text{rad}}_{\text{cp},k+1} \right\|$
  if $J(E^{\text{rad}}_{\text{cp},k}) < \varepsilon$
    return $E^{\text{rad}}_{\text{cp},k}$
    Stop, the algorithm converges to a point in $\mathcal{M} \cap \mathcal{R}$
  else if $\left| J(E^{\text{rad}}_{\text{cp},k+1}) - J(E^{\text{rad}}_{\text{cp},k}) \right| < \varepsilon$ **then**
    The algorithm converges to trap point
    $w_{\mathcal{R},k} = \left(P_{\mathcal{R}}(E^{\text{rad}}_{\text{cp},k-1}) + E^{\text{rad}}_{\text{cp},k-1}\right)/2$
    $w_{\mathcal{M},k} = \left(E^{\text{rad}}_{\text{cp},k} + P_{\mathcal{R}}(E^{\text{rad}}_{\text{cp},k-1})\right)/2$
    $H_k \equiv \left\{ E^{\text{rad}}_{\text{cp}} = w_{\mathcal{R},k} + \lambda\left(w_{\mathcal{M},k} - w_{\mathcal{R},k}\right); \lambda \in \mathbb{R} \right\}$
    Intersects H_k with the two circumferences of radius T_{min} and T_{max}
    Compute λ_r values such that $\left\| w_{\mathcal{R},k} + \lambda_r\left(w_{\mathcal{M},k} - w_{\mathcal{R},k}\right) \right\|^2 = T^2{}_{\text{min/max}}$
    Redefine $E^{\text{rad}}_{\text{cp},k} = w_{\mathcal{R},k} + \lambda_{\text{min}}\left(w_{\mathcal{M},k} - w_{\mathcal{R},k}\right)$: $\lambda_{\text{min}} \equiv \inf\{\lambda_r\}$
    If $\nexists \lambda_r \in \mathbb{R}$, we intersect H_k with $\mathcal{R}$ set by successive projections $P_{\mathcal{R}}$ and P_{H_k}: we redefine $E^{\text{rad}}_{\text{cp},k,l} = w_{\mathcal{R},k}$
    for $l := 0,\ 1,\ 2, \ldots, N_T$ **do**
      $E^{\text{rad}}_{\text{cp},k,l+1} = P_{H_k}\left(P_{\mathcal{R}}\left(E^{\text{rad}}_{\text{cp},k,l}\right)\right)$
      $J\left(E^{\text{rad}}_{\text{cp},k,l}\right) = \left\| P_{\mathcal{R}}\left(E^{\text{rad}}_{\text{cp},k,l}\right) - E^{\text{rad}}_{\text{cp},k,l+1} \right\|$
      if $J(E^{\text{rad}}_{\text{cp},k,l}) < \varepsilon$
        The algorithm converges to a point in $H_k \cap \mathcal{R}$. We redefine $E^{\text{rad}}_{\text{cp},k} = E^{\text{rad}}_{\text{cp},k,l}$
      else if $\left| J(E^{\text{rad}}_{\text{cp},k,l+1}) - J(E^{\text{rad}}_{\text{cp},k,l}) \right| < \varepsilon$ **then**
        The algorithm converges to trap point. We redefine $E^{\text{rad}}_{\text{cp},k} = E^{\text{rad}}_{\text{cp},k,l}$
      end if
    end for
  end if
end for

4. Since $\mathbb{R}^2$ is considered, we define the separating hyperplane H_i as the straight lines which contains the points $w_{\mathcal{R},i}$ and $w_{\mathcal{M},i}$ (i.e. $H_i \equiv \{E^{\text{rad}}_{\text{cp}} = w_{\mathcal{R},i} + \lambda(w_{\mathcal{M},i} - w_{\mathcal{M},i}); \lambda \in \mathcal{R}\}$. Despite orthogonality between H_i and the gradient vector of $\mathcal{R}$ is not guaranteed in the point $P_{\mathcal{R}}(E^{\text{rad}}_{\text{cp},i})$, this definition produces better results when the algorithm is applied. Since the involved sets $\mathcal{M}$ and $\mathcal{R}$ are not convex, the hyperplane H_i is not strictly a separating hyperplane, only locally.
5. The intersection points between H_i and the boundary of $\mathcal{M}$ is obtained in the case of $H_i \cap \mathcal{M} \neq \emptyset$. Since the boundary of $\mathcal{M}$ are two concentric circumferences of T_{min} and T_{max} radius respectively, (i.e. $\|E^{\text{rad}}_{\text{cp}}\|^2 = (\text{Re}(E^{\text{rad}}_{\text{cp}}))^2 + (\text{Im}(E^{\text{rad}}_{\text{cp}}))^2 = T^2_{\text{min/max}}$) then it is possible that there exist two points of intersection with boundary of $\mathcal{M}$, belonging each point to each circumference. In that case, we select the intersection point whose distance with $w_{\mathcal{R},i}$ is minimum. The selected point will be used as initial point $E^{\text{rad}}_{\text{cp},i}$ in step 3.
6. If $H_i \cap \mathcal{M} = \emptyset$ with H_i obtained from $w_{\mathcal{R},i}$ and $w_{\mathcal{M},i}$, then H_i acts as separating hyperplane between $P_{\mathcal{R}}(E^{\text{rad}}_{\text{cp},i-1})$ and $\mathcal{M}$ set. So, we intersects H_i with $\mathcal{R}$ set by successive projections $P_{\mathcal{R}}$ and P_{H_i} as it is described in [18] (see the algorithm shown in Table 3 for more details). The projection on H_i is the conventional projections from a point to a straight line.

Table 3 and Fig. 6 show the pseudocode and flowchart of adapted algorithm respectively:

Fig. 7 shows two cases for the extended algorithm. A first case where $\mathcal{R}$ set is inside the external boundary of $\mathcal{M}$ set (i.e. $\mathcal{R}$ is inside the circumference of T_{max} radius), and a second case where part of $\mathcal{R}$ set is outside to external boundary of $\mathcal{M}$ set (i.e. part of $\mathcal{R}$ is outside the circumference of T_{max} radius).

We would like to point out that, in second case (see Fig. 7(b)), the set $\mathcal{M}$ behaves like a convex set. The reason is because, in this case the algorithm not use interior points of $\mathcal{M}$ set, only points of exterior boundary (i.e. points which belongs to the set $\{E^{\text{rad}}_{\text{cp}} \in \mathbb{C} : (\text{Re}(E^{\text{rad}}_{\text{cp}}))^2 + (\text{Im}(E^{\text{rad}}_{\text{cp}}))^2 = T^2_{\text{min/max}}\}$ are only used). So, in this case $H_i \cap \mathcal{M} = \emptyset$ and according with pass 6, we intersects H_i with $\mathcal{R}$ set by successive projections $P_{\mathcal{R}}$ and P_{H_i} as it is described in [18]. Other important point in the proposed algorithm is that, once the trap point is leaved, the intersection between H_i and the boundaries of set $\mathcal{M}$ produces acceleration of the algorithm with respect to a successive projections of the operators $P_{\mathcal{M}}$ and $P_{\mathcal{R}}$. In this way, the proposed algorithm is not only useful for leaving the trap point, but also for accelerating with respect to successive projection scheme.

4.2. Algorithm based on decomposition method in polar cones

Prior to describing the algorithm based on decomposition in polar cones, let us introduce required concepts.

Definition 4. A non-empty set K in a vector space is called a cone if $x \in K$ imply that $\alpha x \in K\ \forall \alpha \geq 0$. If in addition K is convex, then K is called convex cone.

Definition 5. Let us K a cone in a Hilbert Space $\mathcal{H}$, then the polar cone of K, denoted by K^o, is given by $K^o \equiv \{x \in \mathcal{H} : \langle x, y\rangle \leq 0\ \forall y \in K\}$.

From Definition 5 we can note that K^o is closed convex cone and that if K is close convex cone then $(K^o)^o = K$. Please, note that Definition 4 define a closed convex cone in more general sense than conventional cone definition. For example, a half-line is closed convex cone according with Definition 4. In this case, the closed convex polar cone is the half-plane whose boundary is a line orthogonal to the previous half-line and that intersects it at its vertex. Moreover, decomposition in polar cones known as Moreau's theorem will be required:

Theorem 2. *Let us $x, y, z \in \mathcal{H}$ Hilbert Space and $K \subseteq \mathcal{H}$. If K is a closed convex cone, then $\left[z = x + y,\ with\ x \in K, y \in K^o,\ and\ \langle x, y\rangle = 0\right]$ if and only if $\left[x = P_K(z)\ and\ y = P_{K^o}(z)\right]$.*

Once Definition 4, 5 and Theorem 2 are stated, the proposed algorithm based on decomposition method in polar cones of [18] can be described. Let us consider a non-convex set, A, and other convex set, B, and their projector operators P_A and P_B, and let us consider a trap point on A set. This algorithm is recommended in order to leave a trap point, x_T, when trap point is reached by successive projections. The basic idea consists in making a separating hyperplane, H_0, close to trap point (in similar manner as was described in Section 4.1). Since separating hyperplane, H_0, is a closed convex set, the polar cone $(H_0)^o$ is defined. After that, decomposition in polar cones based on Moreau's theorem (Theorem 2) is applied such as $x_T = P_{H_0}(x_T) + P_{(H_0)^o}(x_T)$. Then the algorithm projects the component $P_{(H_0)^o}(x_T)$ on non-convex set A, $z = P_A(P_{(H_0)^o}(x_T))$. Again decomposition in polar cones is carried out such as $z = P_{H_0}(z) + P_{(H_0)^o}(z)$ and the component $P_{H_0}(z)$ is projected on non-convex set A again, $P_A(P_{H_0}(z))$. It is expected that the distance from x_T to $P_A(P_{(H_0)^o}(x_T))$ is less than the distance from x_T to $P_A(P_{H_0}(z))$ (i.e. $\|x_T - P_A(P_{(H_0)^o}(x_T))\| < \|x_T - P_A(P_{H_0}(z))\|$. So, it is expected that the trap point is leaved. In fact, numerical results with promising results are shown in [18] (see Table 4 of results of experiment 3 in [18]).

We extend the proposed algorithm in [18] to face reflectarray antenna synthesis. The following points describe this extension considering fixed values of u, v:

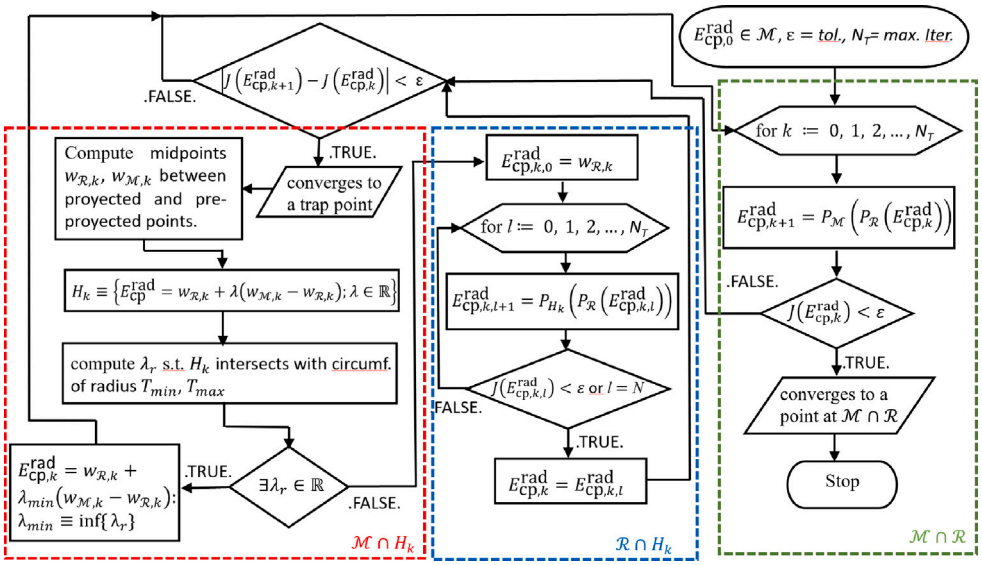

Fig. 6. Flowchart of the algorithm 2 given in Table 3. Three blocks are distinguished: a first block to find $\mathcal{M} \cap \mathcal{R}$, else a second block to find $\mathcal{M} \cap H_k$, else a third block to find $\mathcal{R} \cap H_k$. The initial point for the next iteration is the intersection point into $\mathcal{M} \cap H_k$ or into $\mathcal{R} \cap H_k$.

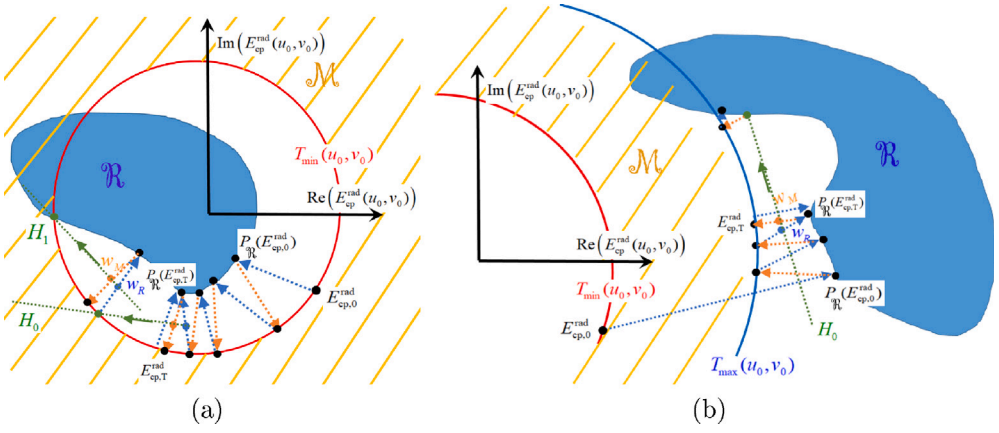

Fig. 7. (a) Extended algorithm based on separating hyperplanes when $\mathcal{R}$ set is inside the external boundary of $\mathcal{M}$ set (i.e. $\mathcal{R}$ is inside the circumference of T_{max} radius); (b) Extended algorithm based on separating hyperplanes when part of $\mathcal{R}$ set is outside the external boundary of $\mathcal{M}$ set (i.e. part of $\mathcal{R}$ is outside the circumference of T_{max} radius).

1. Since $E^{rad}_{cp} = (\mathrm{Re}(E^{rad}_{cp}) + j\mathrm{Im}(E^{rad}_{cp})) \in \mathbb{C}$, we will consider $(\mathrm{Re}(E^{rad}_{cp}), \mathrm{Im}(E^{rad}_{cp})) \in \mathbb{R}^2$ with conventional Euclidean inner product. Moreover, if $(\mathrm{Re}(E^{rad}_{cp}), \mathrm{Im}(E^{rad}_{cp})) \in \mathbb{R}^2$ represents $(\mathrm{Re}(E^{rad}_{cp}) + j\mathrm{Im}(E^{rad}_{cp})) \in \mathbb{C}$, the rotated vector $+\pi/2$, $(-\mathrm{Im}(E^{rad}_{cp}), \mathrm{Re}(E^{rad}_{cp})) \in \mathbb{R}^2$ represents $(j\mathrm{Re}(E^{rad}_{cp}) - \mathrm{Im}(E^{rad}_{cp})) \in \mathbb{C}$.
2. We will consider $\mathcal{M}$ and $\mathcal{R}$ sets defined in (14) and (16). We remember that they are non-convex sets and for this reason, this is an extension of the algorithm.
3. Let us $E^{rad}_{cp,i} = P_{\mathcal{M}}(P_{\mathcal{R}}(E^{rad}_{cp,i-1})) = E^{rad}_{cp,T} \in \mathcal{M}$ a trap point. We define $w_{\mathcal{R},i} = (P_{\mathcal{R}}(E^{rad}_{cp,i-1}) + E^{rad}_{cp,i-1})/2$ and $w_{\mathcal{M},i} = (E^{rad}_{cp,i} + P_{\mathcal{R}}(E^{rad}_{cp,i-1}))/2$.
4. We define the separating hyperplane H_i as the straight lines which contains the points $w_{\mathcal{R},i}$ and $w_{\mathcal{M},i}$ (i.e. $H_i \equiv \{E^{rad}_{cp} = w_{\mathcal{R},i} + \lambda(w_{\mathcal{M},i} - w_{\mathcal{M},i}); \lambda \in \mathcal{R}\}$. Since the involved sets $\mathcal{M}$ and $\mathcal{R}$ are not convex, the hyperplane H_i is not strictly a separating hyperplane, only locally.
5. We define $(H_i)^o$ as the orthogonal straight line to H_i that intersects with H_i in the point q_i such that $\|E^{rad}_{cp,i} - w_{\mathcal{M},i}\| = \|q_i - w_{\mathcal{M},i}\|$ (i.e. $(H_i)^o \equiv \{E^{rad}_{cp} = q_i + j\lambda(w_{\mathcal{M},i} - w_{\mathcal{R},i}); \lambda \in \mathbb{R}\}$).
6. $E^{rad}_{cp,i}$ is decomposed in polar cones such as $E^{rad}_{cp,i} = P_{H_i}(E^{rad}_{cp,i}) + P_{(H_i)^o}(E^{rad}_{cp,i})$. Then the algorithm projects the component $P_{(H_i)^o}(E^{rad}_{cp,i})$ on non-convex set $\mathcal{R}$, $z_i = P_{\mathcal{R}}(P_{(H_i)^o}(E^{rad}_{cp,i}))$. Again decomposition in polar cones is carried out such as $z_i = P_{H_i}(z_i) + P_{(H_i)^o}(z_i)$ and the component $P_{H_i}(z_i)$ is projected on non-convex set $\mathcal{R}$ again, $P_{\mathcal{R}}(P_{H_i}(z_i))$. In this point, we redefine $E^{rad}_{cp,i}$ as $P_{\mathcal{R}}(P_{H_i}(z_i))$ and we start from pass 3 again.

Table 4 and Fig. 8 show the pseudocode and flowchart of adapted algorithm respectively:

Fig. 9 shows two cases for the extended algorithm. A first case where $\mathcal{R}$ set is inside the external boundary of $\mathcal{M}$ set (i.e. $\mathcal{R}$ is inside the circumference of T_{max} radius), and a second case where part of $\mathcal{R}$ set is outside the external boundary of $\mathcal{M}$ set (i.e. part of $\mathcal{R}$ is outside the circumference of T_{max} radius).

Again we would like to point out that, in second case (see Fig. 9(b)), $\mathcal{M}$ set behaves like a convex set because of same reason described in previous section. We would not like to end this subsection without emphasizing the use of the proposed algorithm to leave the trap point (it is not expected that this algorithm works to converge to the intersection of the involved sets, only to leave the trap point). In this way, it is expected that, a hybridized algorithm can produce better results than each algorithm separately. This hybridized algorithm has been implemented: first with iterations of the algorithm based on decomposition method in polar cones and after, with iterations of the algorithm based on separating hyperplanes.

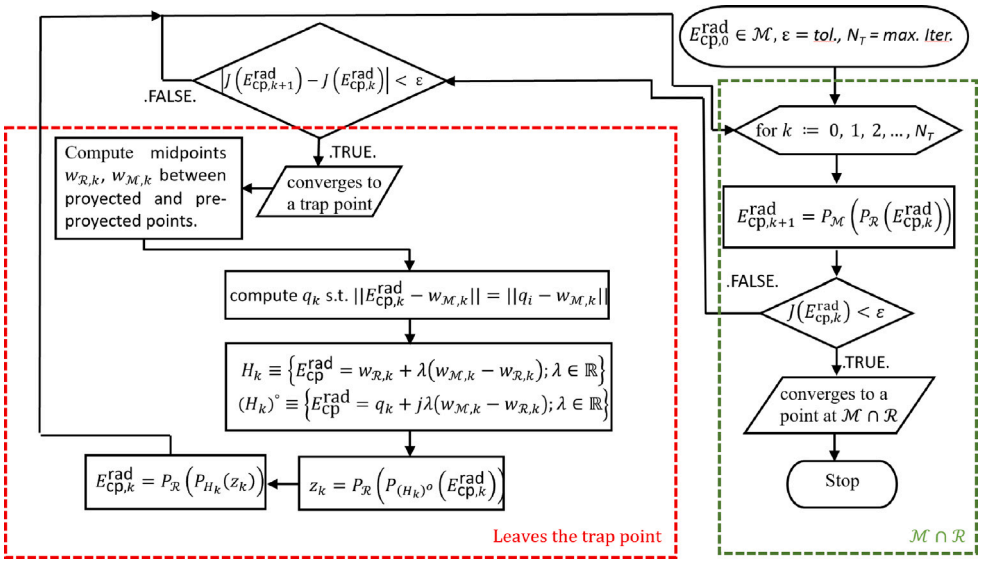

Fig. 8. Flowchart of the algorithm 3 given in Table 3. Two blocks are distinguished: a first block to find $\mathcal{M} \cap \mathcal{R}$, else a second block to leave the trap point. The initial point for the subsequent iteration is that obtained to leave the trap point.

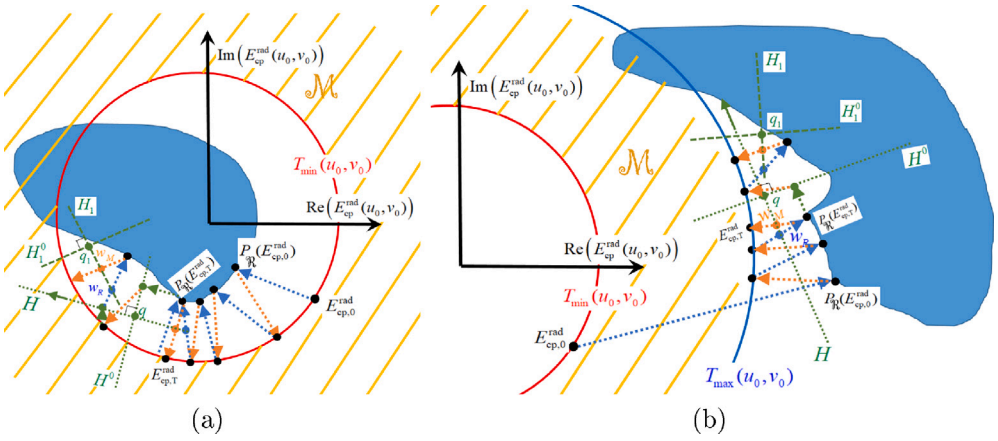

Fig. 9. (a) Extended algorithm based on decomposition method in polar cones when $\mathcal{R}$ set is inside the external boundary of $\mathcal{M}$ set (i.e. $\mathcal{R}$ is inside the circumference of T_{max} radius); (b) Extended algorithm based on separating hyperplanes when part of $\mathcal{R}$ set is outside the external boundary of $\mathcal{M}$ set (i.e. part of $\mathcal{R}$ is outside the circumference of T_{max} radius).

5. Results

A comparison of results obtained by each algorithm, von Neumann's algorithm (see Table 2), the algorithm based on separating hyperplanes (see Table 3), the algorithm based on decomposition method in polar cones (see Table 4), and hybridized algorithm will be shown in this section. So, we will show comparisons of results considering mission requirements for Europe coverage given in Fig. 2 [14].

In Fig. 2(a) contour of Europe coverage seen from 5° west orbital position is shown while that, in Fig. 2(b) minimum gain requirements in the defined coverage are shown [14]. Two gain regions of 28.5 dBi (interior region with respect to the solid line contour) and 25.5 dBi (interior region limited by the dashed line and solid line contours) are required. So, the minimum required gain $g^{min}_{cp}(u,v)$ is fixed to 28.5 dBi and 25.5 dBi in each region respectively. In the outer coverage region a maximum of 0 dBi is required. So, the maximum required gain $g^{max}_{cp}(u,v)$ is fixed to 0 dBi in the outer coverage region. Note that, there is not a maximum required gain $g^{max}_{cp}(u,v)$ inside coverage region and neither a minimum required gain $g^{min}_{cp}(u,v)$ outside coverage region. All these requirements are required at the work frequency given by 12.1 GHz [14]. From all these restrictions, the maximum and minimum values of the magnitude of the co-polar component of the radiated electric field, $T_{min}(u,v)$ and $T_{max}(u,v)$ respectively, can be computed using (12) and (13).

To fulfill previous requirements, we consider the following geometry properties and illumination proposed in [14]. The reflectarray consists of an elliptical flat panel with axes 1036 × 980 mm^2. The total number of elements is 4068 distributed in 74 columns and 70 rows of 14 × 14 mm^2 of size cell. The center phase of the feed-horn is located in the point $(-302, 0, 898)$ mm with respect to the reference system located on the center of the reflectarray (see Fig. 1). The feed-horn is selected to provide −16 dB of edge illumination with respect to the maximum of illumination on the center of the reflectarray panel. In order to computed the tangential components of the incident electric field, the radiation pattern of the feed-horn has been modeled with $\cos^q(\theta)$ model [3,22] with $q = 17$ at 12.1 GHz.

We launch the four algorithms: von Neumann's algorithm (algorithm 1 given in Table 2), the algorithm based on separating hyperplanes (algorithm 2 given in Table 3), the algorithm based on decomposition method in polar cones (algorithm 3 given in Table 4), and hybridized algorithm of algorithm 2 and algorithm 3. The initial point used for all algorithms is given by the co-polar component of the radiated field $E^{rad}_{cp,0}(u,v) = T_{min}(u,v)$ and the tolerance ϵ is fixed to 0.1. The hybridized algorithm implemented consist of applying the

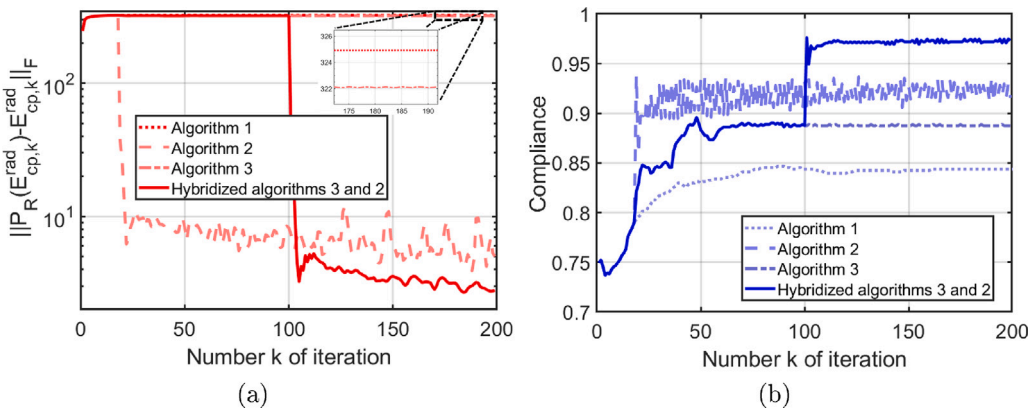

Fig. 10. (a) Frobenius norm of the difference between projected and pre-projected co-polar components of radiated electric field versus number of iteration (i.e. $J(E^{\text{rad}}_{\text{cp},k}) = \|P_{\mathcal{R}}(E^{\text{rad}}_{\text{cp},k}) - E^{\text{rad}}_{\text{cp},k}\|$); (b) Fraction of the radiation pattern which satisfies the mission requirements (i.e. the fraction of radiation pattern which satisfies $T_{\min} \leq \left|E^{\text{rad}}_{\text{cp}}\right| \leq T_{\max}$).

Table 4
AGP based on decomposition method in polar cones.

Algorithm 3: AGP based on decomposition method in polar cones

1:Require $E^{\text{rad}}_{\text{cp},0} \in \mathcal{M}$, ε = tolerance, N_T := maximum number of iterations
2:**for** $k := 0, 1, 2, \ldots, N_T$ **do**
3: $E^{\text{rad}}_{\text{cp},k+1} = P_{\mathcal{M}}\left(P_{\mathcal{R}}\left(E^{\text{rad}}_{\text{cp},k}\right)\right)$
4: $J\left(E^{\text{rad}}_{\text{cp},k}\right) = \left\|P_{\mathcal{R}}\left(E^{\text{rad}}_{\text{cp},k}\right) - E^{\text{rad}}_{\text{cp},k+1}\right\|$
5: **if** $J(E^{\text{rad}}_{\text{cp},k}) < \varepsilon$
6: **return** $E^{\text{rad}}_{\text{cp},k}$
7: Stop, the algorithm converges to a point in $\mathcal{M} \cap \mathcal{R}$
8: **else if** $\left|J(E^{\text{rad}}_{\text{cp},k+1}) - J(E^{\text{rad}}_{\text{cp},k})\right| < \varepsilon$ **then**
9: The algorithm converges to trap point
10: $w_{\mathcal{R},k} = \left(P_{\mathcal{R}}(E^{\text{rad}}_{\text{cp},k-1}) + E^{\text{rad}}_{\text{cp},k-1}\right)/2$
11: $w_{\mathcal{M},k} = \left(E^{\text{rad}}_{\text{cp},k} + P_{\mathcal{R}}(E^{\text{rad}}_{\text{cp},k-1})\right)/2$
12: Compute q_k such that $\left\|E^{\text{rad}}_{\text{cp},k} - w_{\mathcal{M},k}\right\| = \|q_k - w_{\mathcal{M},k}\|$
13: $H_k \equiv \left\{E^{\text{rad}}_{\text{cp}} = w_{\mathcal{R},k} + \lambda\left(w_{\mathcal{M},k} - w_{\mathcal{R},k}\right); \lambda \in \mathbb{R}\right\}$
14: $(H_k)^o \equiv \left\{E^{\text{rad}}_{\text{cp}} = q_k + j\lambda\left(w_{\mathcal{M},k} - w_{\mathcal{R},k}\right); \lambda \in \mathbb{R}\right\}$
15: Compute $z_k = P_{\mathcal{R}}(P_{(H_k)^o}\left(E^{\text{rad}}_{\text{cp},k}\right))$
16: Compute $E^{\text{rad}}_{\text{cp},k} = P_{\mathcal{R}}(P_{H_k}(z_k))$
18: **end if**
19:**end for**

algorithm 3 (based on decomposition in polar cones) during the first 100 iterations, and after applying the algorithm 2 (based on separating hyperplanes) during the rest of iterations.

The size of the cell $a = b = 14$ mm and values of $M = N = 2^9$ has been used in the partition of the S_{RA}. In order to quantify the distance between projected and pre-projected points for all discrete values of u and v, let us consider a matrix $(E^{\text{rad}}_{\text{cp},k})$ with $M \times N$ entries. The matrix entries are evaluations of $E^{\text{rad}}_{\text{cp},k}$ for discrete values of u and v in the coverage region. We define the norm $\|E^{\text{rad}}_{\text{cp},k}\|^2$ as Frobenius norm of the matrix $(E^{\text{rad}}_{\text{cp},k})$. This definition is motivated because the $\|E^{\text{rad}}_{\text{cp},k}\|^2$ is proportional to known physical magnitude. This known physical magnitude is the power generated by the co-polar component of the radiated electric field $E^{\text{rad}}_{\text{cp},k}$ (i.e. the power is the closed surface integral of the pointing vector in the region inner of closed surface, being the modulus of vector pointing proportional to square of the magnitude of the electric field). So, $J(E^{\text{rad}}_{\text{cp},k}) = \|P_{\mathcal{R}}(E^{\text{rad}}_{\text{cp},k}) - E^{\text{rad}}_{\text{cp},k}\|$ will show the Frobenius norm of the difference $P_{\mathcal{R}}(E^{\text{rad}}_{\text{cp},k}) - E^{\text{rad}}_{\text{cp},k}$ in order to quantify the distance between the projected point and pre-projected point taking into account all discrete values of u and v of the coverage region.

Fig. 10(a) shows the Frobenius norm of the difference between projected and pre-projected co-polar components of radiated electric field obtained by the different algorithms versus number of iteration. We can see that the algorithm 1 (von Neumann's method) provides a value of Frobenius norm of the difference between projected and pre-projected point equal to 370 from 50 iterations of the algorithms. This value of the Frobenius norm is drastically reduced (37 times less) by the algorithm 2 (separating hyperplanes). So, the projected and pre-projected points get closer. Since lower values than previous values obtained by von Neumann's method of the Frobenius norm are achieved by algorithm 2, the von Neumann's method converges to trap point. The algorithm 3 (decomposition method in polar cones) produces slightly lower values of the Frobenius norm than obtained values by algorithm 1 (the projected and pre-projected points are slightly closer). This fact is expected since this method is prepared to leave the trap point and not to converge to the intersection of the sets. Finally, the hybridized algorithm provides the lowest value of Frobenius norm (close to 100 times less than algorithm 1 results – von Neumann method –) from 100 iterations (just when the separating hyperplanes method is activated). On the other hand, Fig. 10(b) shows the fraction of the radiation pattern which satisfies the mission requirements (i.e. the fraction of radiation pattern which satisfies $T_{\min} \leq \left|E^{\text{rad}}_{\text{cp}}\right| \leq T_{\max}$). We can see that the algorithm 1 (von Neumann's method) provides values of compliance lower than 85 per cent of the whole radiation pattern. The algorithm 2 provides very oscillating values of compliance higher than 90 per cent. The algorithm 3 provides values of compliance slightly lower than 90 per cent. Finally, when hybridized algorithm is applied, values of compliance are significantly incremented from the compliance values provided by algorithm 3 (when decomposition method in polar cones is activaded) until 98 per cent of the radiation pattern from 100 iterations (just when the separating hyperplanes method is activated). In this way, the proposed hybridized algorithm provides best results of reduction of distance between projected and pre-projected points involving significant improvements of the compliance.

Fig. 11(a) and (b) show the radiation pattern of the gain of the co-polar radiated electric field with respect to the minimum required gain $g^{\min}_{\text{cp}}(u, v)$ provided in the final iteration (k=200) by the algorithm 1 (von Neumann method) and the hybridized algorithm respectively. Note that the values of difference of gain upper than 0 dB are limited to 0 dB in order to easily identify the regions where the mission requirements are not satisfied (i.e. to identify regions where the minimum required gain $g^{\min}_{\text{cp}}(u, v)$ is upper than the resultant gain of the co-polar radiated electric field generated by the reflectarray antenna). We can see that, while the von Neumann method provides roughly five regions with non-compliance inside coverage regions, the results provided by hybridized algorithm only show two small non-compliance regions at the edges of the coverage regions. So, the results provided by the hybridized algorithm are much better than the results provided by von Neumann method.

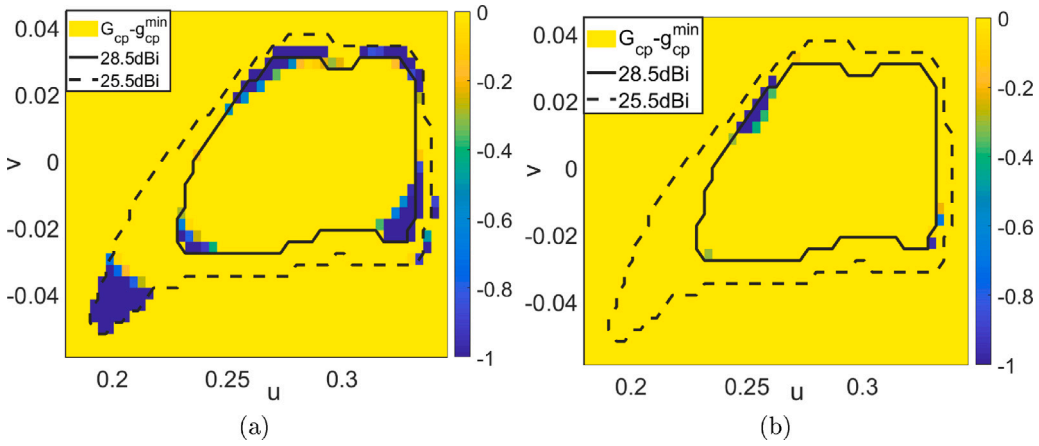

Fig. 11. Radiation pattern of the gain of the co-polar radiated electric field with respect to the minimum required gain $g_{cp}^{min}(u, v)$ provided in the final iteration (k=200) (a) by the algorithm 1 (von Neumann method) and (b) by the hybridized algorithm.

6. Conclusions

In this work phase-only synthesis of satellite reflectarray antennas using Intersection Approach for two sets has been reviewed: the set $\mathcal{M}$ of radiated electric fields which satisfy the mission requirements, and the set $\mathcal{R}$ of radiated electric fields which can be generated by the reflectarray. Non-convexity of $\mathcal{M}$ and $\mathcal{R}$ sets has been revealed. When any involved sets is not convex, convergence to intersections points or points of each set that are at the minimum distance is not guaranteed by method POCS (for example by von-Neumann's method). When two non-convex sets are considered, it is possible to detect trap points where local minimum of distance between involved sets is found.

Two different algorithms proposed in [18] to leave trap points are rescued. These two proposed algorithms are: algorithm based on separating hyperplanes and algorithm based on decomposition method in polar cones. According with [18], it is expected that the algorithm based on separating hyperplanes generates a convergent sequence to a point of intersections of the sets. On the contrary, in [18] it is expected that the algorithm based decomposition method in polar cones works to leave the trap point. So, in this work hybridized algorithm is proposed. The hybridized algorithm implemented consist of applying the algorithm based on decomposition in polar cones during the first iterations (to leave the trap point), and after applying the algorithm based on separating hyperplanes during the rest of iterations.

A comparison of results obtained by each algorithm, von Neumann's algorithm (see Table 2), the algorithm based on separating hyperplanes (see Table 3), the algorithm based on decomposition method in polar cones (see Table 4), and hybridized algorithm have been shown with requirements for Europe coverage given in Fig. 2 [14]. In order to quantify the distance between projected and pre-projected points for all discrete values of u-v diagram of radiation pattern, we have used the Frobenius norm for the evaluation of this distance. So, the Frobenius norm between projected and pre-projected points have been compared with respect to the number of iteration with the four algorithms. In this comparison the hybridized algorithm provides the lowest value of Frobenius norm with reductions of 100 times less with respect to those obtained by algorithm 1. Also fraction of the radiation pattern which satisfies the mission requirements have been computed with respect to the number of iteration with the four algorithms. Improvements of compliance reach 98 per cent using hybridized algorithm. So, All results shown that the proposed hybridized algorithm provides significant improved results with respect to those obtained by conventional von Neumann algorithm proposed so far in the literature for the only-phase synthesis of satellite reflectarray antennas.

CRediT authorship contribution statement

Rafael Florencio: Writing – review & editing, Writing – original draft, Validation, Software, Methodology, Investigation, Formal analysis, Conceptualization. **René Escalante:** Writing – review & editing, Writing – original draft, Validation, Software, Methodology, Investigation, Formal analysis, Conceptualization.

Declaration of competing interest

The authors declare that they have no known competing financial interests or personal relationships that could have appeared to influence the work reported in this paper.

Data availability

No data was used for the research described in the article.

Acknowledgment

"Funding for open access charge: Universidad de Jaén". Moreover, We would like to thank two anonymous referees for useful suggestions.

References

[1] Garcia H, Barraud P, Buralli B, Bouvin C, Martel B, Vacarella M, et al. Design and testing of large telecommunication satellites antennas. JINA 2002.
[2] Imbriale A, Gao S, Boccia L. Space antenna handbook. John Wiley and Sons; 2012.
[3] J. Huang, Encinar JA. Reflectarray antennas. Piscataway, NJ, USA: IEEE Press/Wiley; 2008.
[4] Encinar JA. Design of two-layer printed reflectarrays using patches of variable size. IEEE Trans Antennas Propag 2001;49:1403–10.
[5] Florencio R, Encinar JA, Boix RR, Losada V, Toso G. Reflectarray antennas for dual polarization and broadband telecom satellite applications. IEEE Trans Antennas and Propagation 2015;63(4):1234–46.
[6] Encinar JA, Zornoza JA. Broadband design of three-layer printed reflectarrays. IEEE Trans Antennas and Propagation 2003;51(7):1662–4.
[7] Carrasco E, Encinar JA, Barba M. Bandwidth improvement in large reflectarrays by using true-time-delay. IEEE Trans Antennas Propag 2008;56:2496–503.
[8] Bucci OM, Elia GD. Power synthesis of reconfigurable conformal arrays with phase - only control. IEE Proc - Microw Antennas Propag 1998;145(1):131–6.
[9] Kautz GM. Phase - only shaped beam synthesis via technique of approximated beam addition. IEEE Trans Antennas Propag 1999;47(5):887–94.
[10] Trastoy A, Ares F, Moreno E. Phase - only control of antenna sum and shaped patterns through null perturbation. Antennas Propag Mag 2001;45–54.
[11] Zornoza A. Desarrollo de Técnicas de Diseño para Reflectarrays Impresos Multicapa con Haz Conformado (Phd. Thesis), Madrid, Spain: Department of Electromagnetic and Circuit Theory, Polytechnic University of Madrid; 2004.
[12] Bucci OM, Franceschetti G, Mazzarella G, Panariello G. Intersection approach to array pattern synthesis. IEE Proc 1990;137(6):349–57, pt. H.

[13] Bucci OM, D'Elia G, Mazzarella G, Panariello G. Antenna pattern synthesis: a new general approach. Proc IEEE 1994;82:358–71.
[14] Encinar JA, Datashvili LSh, Zornoza JA, Arrebola M, Sierra-Castañer M, Besada-Sanmartín JL, et al. Dual-polarization dual-coverage reflectarray for space applications. IEEE Trans Antennas Propag 2006;54(10):2827–37.
[15] Escalante R, Raydan M. Alternating projection methods. Philadelphia: Society for Industrial and Applied Mathematics; 2011.
[16] Neumann John von. Functional operators. In: Vol II. geometry of orthogonal spaces. Annals of math. studies 22, Princeton, NJ: Princeton University Press; 1950.
[17] Cheney W, Goldstein A. Proximity maps for convex sets. Proc Amer Math Soc 1959;10:448–50.
[18] Andrade M, Escalante R, Espitia R. Some convergence strategies for the alternating generalized projections method. Bull Comput Appl Math 2013;1(2).
[19] Combettes P, Trussell HJ. Method of successive projections for finding a common point of sets in metric spaces. J Optim Theory Appl 1990;67:487–507.
[20] Chrétien S, Bondon P. Cyclic projection methods on a class of nonconvex sets. Numer Funct Anal Optim 1996;17:37–56.
[21] Bauschke HH, Phan HM, Wang X. The method of alternating relaxed projections for two nonconvex sets. Vietnam J Math 2014;42:421–50.
[22] Lo YT, Lee SW. Antenna handbook. Vol. I. antenna fundamentals and mathematical techniques. Van Nostrand Reinhold; 1993.
[23] Hansen JE. Spherical near-field measurements. In: IEE electromagnetics wave series 26, Peter Peregrinus Ltd; 1988.
[24] Palomino GP, Encinar JA, Barba M. Method for accurately solving the scattering in planar reflectarrays under an ar-bitrary excitation. In: 6th European conference on antennas and propagation, EUCAP 2012. 2012, p. 1081–5.
[25] Clark RH, Brown J. Diffraction theory and antennas. Chichester: Ellis Horwood; 1980, p. 85–6.
[26] Pontoppidan K. Technical Description of GRASP8 (TICRA).
[27] De la Rubia V, Zapata J, González MA. Finite element analysis of periodic structures without constrained meshes. IEEE Trans Antennas Propag 2008;56:3020–8.
[28] F. Yang, Rahmat-Samii Y. Electromagnetic band gap structures in antenna engineering. Cambridge, UK: University Press; 2008.
[29] Harrington RF. Field computation by moment methods. New York, NY, USA: McGraw-Hill; 1968.
[30] R. Florencio, Somolinos A, González I, Cátedra MF. BICGSTAB-FFT method of moments with NURBS for analysis of planar generic layouts embedded in large multilayer structures. Electronics 2020;9:1–17.
[31] Press WH, Teukolsky SA, Vetterling WT, Flannery BP. Numerical recipes in FORTRAN. The art of scientific computing, 2nd ed.. Cambridge University Press; 1992.
[32] Ludwig AC. The definition of cross polarization. IEEE Trans Antennas Propag 1973;21(1):116–9.